Sub-Micrometer Mechanochromic Inclusions Enable Strain Sensing in Polymers

Derek J. Kiebala, Robert Style, Dimitri Vanhecke, Céline Calvino, Christoph Weder, and Stephen Schrettl*

Blending different types of polymers with traces of a telechelic macromolecule that is end-functionalized with excimer-forming chromophores affords materials that display a highly sensitive, reversible, and strain-dependent mechanochromic response. Confocal microscopy imaging reveals that the additive forms discrete, phase-separated inclusions in host polymers such as poly(ϵ-caprolactone), poly-isoprene, poly(styrene-*b*-butadiene-*b*-styrene), and different thermoplastic polyurethanes. A comprehensive analysis shows that the mechanochromism of the blends originates from the distortion of the inclusions, which, independent of the additive content and chemical composition of the matrix, deform homogeneously and reversibly in response to the applied macroscopic strain. These findings support the conclusion that such excimer-forming, telechelic macromolecules can be used as universal additives that allow the straightforward fabrication of a wide range of mechanochromic materials.

1. Introduction

Polymers that can signal mechanical deformation through changes of their optical properties are referred to as mechanochromic, and such materials have garnered significant interest due to their potential use for damage reporting and stress-sensing.[1–7] Complex sensor equipment that is employed in load-bearing structural materials could, for example, be replaced by materials that signal fatigue or damage through a visually discernible color change.[8,9] Approaches to impart polymers with mechanochromic behavior include the integration of responsive molecules that undergo force-induced covalent bond scission (mechanophores),[10–12] the use of structurally colored materials whose interaction with light changes upon deformation of an ordered micro- or nanostructure,[13,14] and the use of non-sacrificial mechanoresponsive motifs such as donor–acceptor pairs, conformationally activated species, or dye aggregates that respond to mechanical stimulation without covalent bond scission.[4,15,16] Materials that display mechanoresponsive luminescence (MRL) appear to be particularly useful for the analysis of deformation processes, since changes in the emission color or intensity can be monitored with high sensitivity by spectroscopic or microscopic techniques, as demonstrated in, e.g., elastomers,[17–23] composite materials,[24,25] hydrogels,[26] and organogels.[27] Among the methods for endowing polymeric materials with an MRL response, physical blending with dyes such as excimer-forming cyano-substituted oligo(*p*-phenylene vinylene)s (OPVs) or perylenes has proven to be particularly straightforward.[5,28,29] The approach generally requires that the dyes form nanometer-sized aggregates, whose formation is aided by nucleation through the crystalline domains in semi-crystalline polymers.[5,30,31] The dye aggregates are disintegrated upon deformation of the polymer, which changes the material's optical properties from excimer- to monomer-dominated emission. In amorphous polymer matrices, limited nucleation and relatively high molecular mobility generally lead to the formation of larger dye crystals that are mechanically inert.[32] It therefore remains difficult to endow, e.g., elastomers and related classes of amorphous polymers with MRL properties, unless the dyes are covalently incorporated[33–35] or contained within protective microcapsules.[24,36,37]

We recently discovered that a telechelic macromolecule composed of a poly(ethylene-*co*-butylene) core functionalized with excimer-forming cyano-OPV moieties at its termini (tOPV) can be used as an additive to impart a wide range of

D. J. Kiebala, D. Vanhecke, C. Weder, S. Schrettl
Adolphe Merkle Institute
University of Fribourg
Fribourg CH-1700, Switzerland
E-mail: stephen.schrettl@tum.de
R. Style
ETH Zürich
Department of Materials
Vladimir-Prelog-Weg 1-5/10, Zurich CH-8093, Switzerland
C. Calvino
University of Freiburg
Freiburg Center for Interactive Materials and Bioinspired Technologies
Georges-Köhler-Allee 105, D-79110 Freiburg, Germany
S. Schrettl
Technical University of Munich
TUM School of Life Sciences
Maximus-von-Imhof-Forum 2, D-85354 Freising, Germany

2304938 (1 of 9)

**ADVANCED
SCIENCE NEWS**

www.advancedsciencenews.com

**ADVANCED
FUNCTIONAL
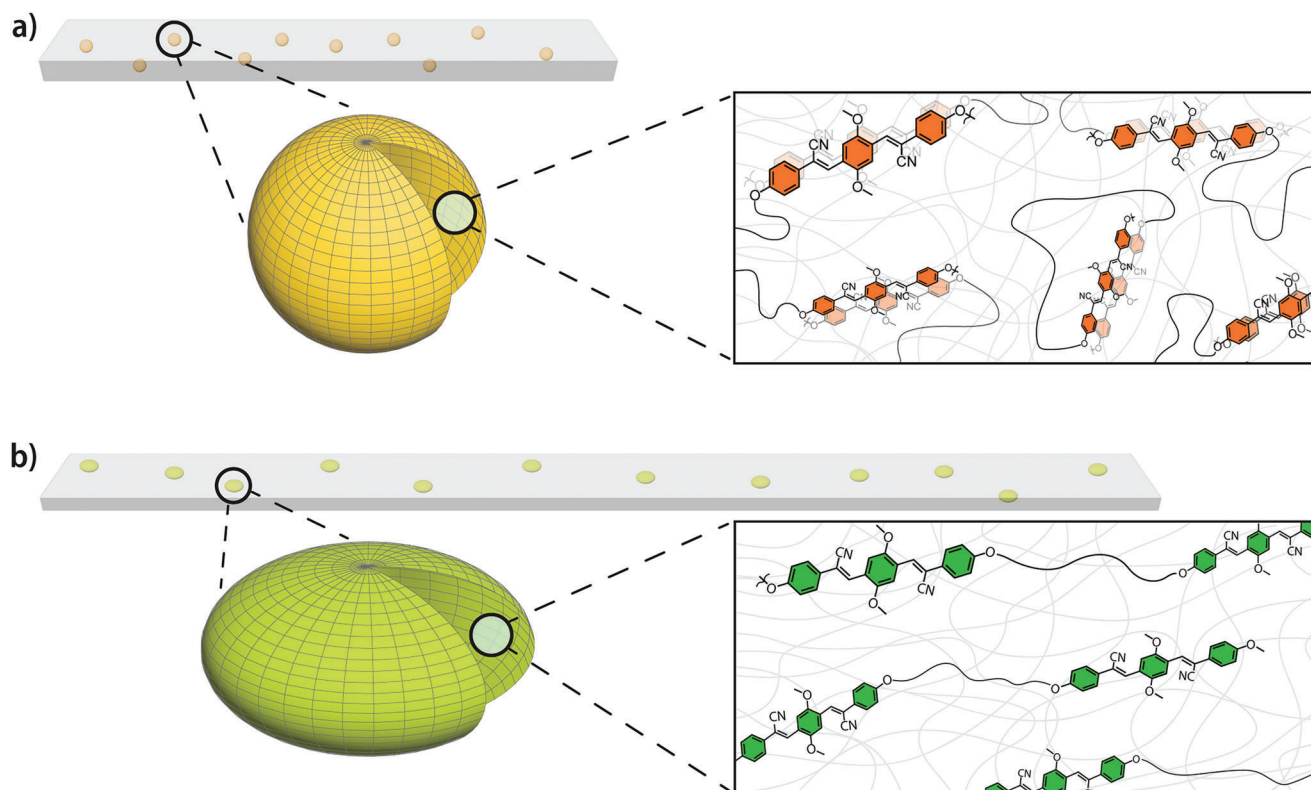MATERIALS**

www.afm-journal.de

Figure 1. Schematic representation of polymers blended with the employed additive, i.e., a telechelic macromolecule with excimer-forming cyano-substituted oligo(p-phenylene vinylene) dyes (tOPV). The additive forms sub-micrometer inclusions, which endow the samples with mechanochromic behavior. Note that the main component of the inclusions is the host polymer. a) Inclusions detected in as-prepared, compression-molded films are spherical and exhibit a relatively high degree of excimer emission, indicating extensive aggregation of the dyes. b) Applying tensile strain to the films deforms the inclusions, which in turn leads to the dissociation of a significant fraction of the aggregated dyes. The result is a distinct change in the emission color of the inclusions, and hence of the blend films.

different semi-crystalline and amorphous polymer matrices with a highly sensitive MRL behavior, including poly(ϵ-caprolactone) (PCL), polyisoprene (PI), poly(styrene-b-butadiene-b-styrene) (SBS), and different thermoplastic polyurethanes.[17,20] For example, blends of a commercial, amorphous polyurethane (PU) elastomer containing as little as 0.25 wt.% of the tOPV additive (number-average molecular weight, $M_n = 4500$ g mol^{-1}, tOPV weight fraction ≈19%) were found to display a reversible MRL response, while samples of the same PU blended with a small-molecule aggregachromic dye showed no response.[20] In situ fluorescence spectroscopy experiments with PU films blended with tOPV were carried out during tensile deformation. The recorded spectra revealed that deformation causes dye aggregates to dissociate, as indicated by strain-correlated changes of the monomer and excimer emission intensities. The MRL response is characterized by an exceptionally low onset strain of only 5%, closely follows the applied strain, and is reversible over multiple deformation and relaxation cycles.[20]

Here, we report a mechanistic study that elucidates how a macromolecular additive bestows different host polymers with mechanochromic characteristics and provide insights about the generality of the approach. The characterization of blend films containing the additive by high-resolution confocal laser scanning microscopy (CLSM) reveals the formation of emissive inclusions at the sub-micrometer scale in all polymer matrices investigated. CLSM data collected in situ during uniaxial deformation experiments unambiguously show that the distortion of the inclusions is responsible for the MRL response of such polymer blends (**Figure 1**). Quantitative image analysis was employed to determine the composition and mechanical properties of the phase-separated inclusions, revealing the latter to be elastic, highly deformable, and largely comprised of the matrix polymer. The stress–strain field inside the inclusions was found to be uniform upon bulk sample deformation, which is in good agreement with the response expected for elastic inclusions in polymeric matrices. We show that the transfer of bulk forces to the inclusions gives rise to the observed linear correlation of the fluorescence signal with the applied strain and also the exceptionally low onset of the MRL response. Our findings suggest that the use of tOPV and similar MRL additives may serve as a general path toward technologically relevant mechanoresponsive materials.

2. Results and Discussion

Films of blends of different polymers with varying amounts (0.25–10 wt.%) of the tOPV additive ($M_n = 4500$ g mol^{-1}) were prepared by co-dissolving the components in tetrahydrofuran (THF), solvent-casting, drying, and, unless otherwise noted, compression-molding as previously reported (see Figure S1, Supporting Information for details).[20] On account of its
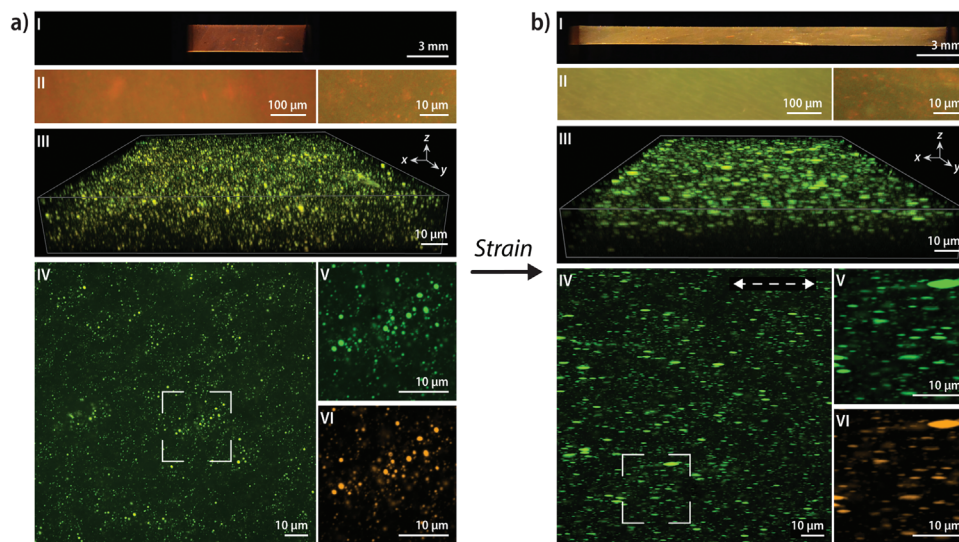
ADVANCED
SCIENCE NEWS
www.advancedsciencenews.com

ADVANCED
FUNCTIONAL
MATERIALS
www.afm-journal.de

Figure 2. Images of a PU/tOPV film a) before and b) after uniaxial extension to 200% strain. I) Photographs of a PU/tOPV (0.25 wt.%) film under UV light illumination (λ_{ex} = 365 nm). II) Fluorescence microscopy images (λ_{ex} = 345 nm) of the center of the film. III–VI) CLSM images (λ_{ex} = 458 nm) of a PU/tOPV (1 wt.%) film at (a) 0% and (b) 200% strain. (III) 3D images (overlay of the monomer and excimer channels) of the top 20 μm of the film. IV–VI) 2D images of the film acquired at a depth of ca. 6 μm showing the emission from IV) 461–725 nm, as well as V) the monomer emission channel (λ_{em} = 461–525 nm) and VI) the excimer emission channel (λ_{em} = 550–725 nm) for the area indicated by the white square.

elastic behavior that allows for reversible deformation, a thermoplastic polyurethane elastomer was chosen for in-depth studies (PU/tOPV), while blends with poly(ϵ-caprolactone) (PCL/tOPV), polyisoprene (PI/tOPV), and poly(styrene-*b*-butadiene-*b*-styrene) (SBS/tOPV) were characterized to ascertain the generality of the mechanism (vide infra). Macroscopically, as-prepared, stress-free PU/tOPV films with as little as 0.25 wt.% of the additive show a homogeneous orange emission color when illuminated with UV light (λ_{ex} = 365 nm; **Figure 2a[I]**), which indicates that a majority of the dyes have formed aggregates that display excimer emission. The formation of tOPV aggregates is corroborated by the yellow-orange appearance of the films under ambient light (Figure S2, Supporting Information), by microscopy images showing enhanced blue-light absorbance of films with higher tOPV content (Figures S3 and S4, Supporting Information), and by solid-state UV–vis spectra showing that the absorbance of samples with high tOPV content closely matches that of neat, fully aggregated tOPV (Figure S5, Supporting Information).[17,38] Fluorescence microscopy imaging with a magnification of up to 100-fold indicates some variation of the emission color throughout the films (Figure 2a[II]), while high-resolution imaging by means of CLSM reveals that the PU/tOPV (0.25–10 wt.%) blend films feature uniformly dispersed, phase-separated inclusions that show the characteristic tOPV emission (Figure 2a[III–VI]; Figures S6–S10, Supporting Information).[17,20] Split-channel imaging was carried out, with one channel (461–525 nm) capturing predominantly monomer-based emission, while the second channel (550–725 nm) was chosen to collect the excimer emission (Figure 2a[V,VI]; Figure S6, Supporting Information). The images thus recorded confirm that the inclusions feature both monomer as well as excimer emission, which is in stark contrast to the neat tOPV additive that exclusively displays excimer emission.[17] While CLSM images of solvent-cast PU/tOPV films show mostly inhomogeneous fluorescent structures (Figure S11, Supporting Information), cooling from the melt yields smooth, well-defined inclusions (Figure 2a[III–VI]), which indicates that their formation is governed by a liquid–liquid phase separation process between the additive and matrix components.[39]

A PU/tOPV blend containing inclusions with high brightness (1.0 wt.%) was selected for detailed analyses by 3D CLSM imaging. The micrographs show a dense array of inclusions throughout the entire film (Figure 2a[III]), with most having apparent radii <500 nm (vide infra). The variations in distribution density appear to be the result of imperfect mixing (Figure 2a[IV]; Figure S8, Supporting Information), while the elongated appearance of individual inclusions is an artifact arising from an inherently lower resolution in the axial (z) dimension compared to the lateral (x,y) dimensions (Figure 2a[III]).[40] Indeed, 2D CLSM images recorded with the same PU/tOPV film that was oriented at an angle of 0°–90° with respect to the microscope objective both show inclusions with a median circularity >0.99 (Figure S12, Supporting Information), confirming that the sub-micrometer inclusions are spherical. The sphericity of the inclusions is further corroborated by atomic force microscopy (AFM) images of PU/tOPV (10 wt.%) samples, which reveal hemispherical protrusions at the surface of the films featuring sizes similar to those observed by CLSM imaging (Figure S13, Supporting Information). To quantitatively assess the fluorescence properties of the inclusions (see below for a discussion of their composition), a comparison of the emission intensities between split-channel micrographs was performed after background subtraction to isolate individual inclusions. The intensity ratio of the signals recorded for the two channels, henceforth referred to as the monomer-to-excimer emission intensity ratio (I_M/I_E), was determined by calculating the I_M/I_E ratio for individual inclusions and averaging these values over the entire population of inclusions in a sample. Notably, photo-bleaching was found to occur during image
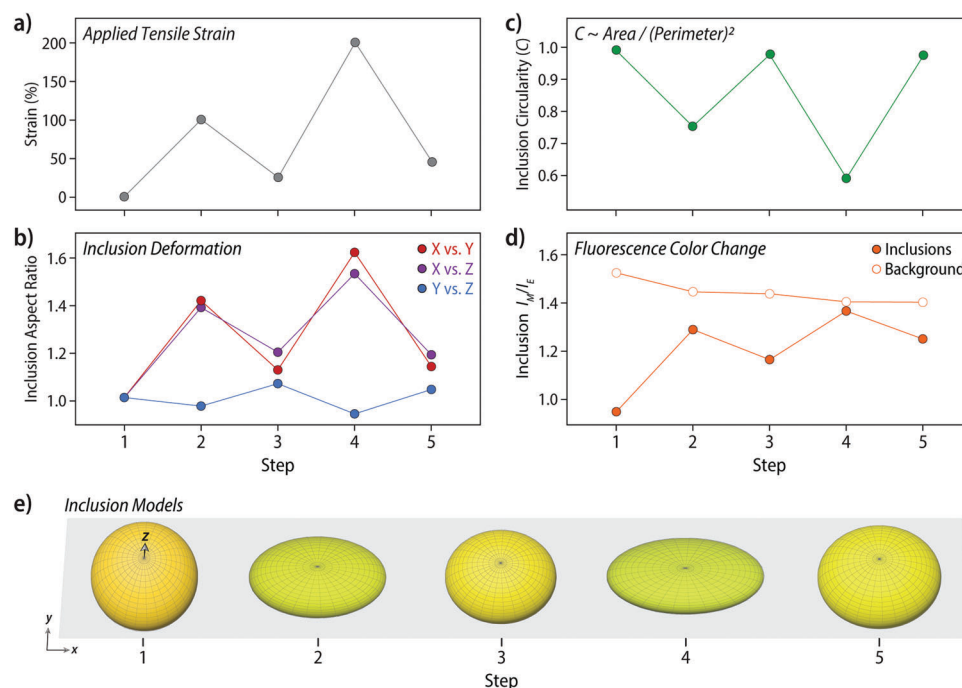
Figure 3. a) Strain of a PU/tOPV (1 wt.%) film induced in two consecutive stretch-release cycles. Step 1 indicates the initial unstretched film (i.e., 0% strain), steps 2–4 the first and second deformed states, and steps 3–5 the first and second relaxed states; for the latter, the sample was allowed to relax for 10 min to reach the indicated strain. b) Average change of the inclusions' aspect ratio for all inclusions detected (150 nm $< r_i <$ 5 µm) in 3D CLSM images of the film for each deformation and relaxation step. r_i refers to the initial spherical radii of the inclusions before deformation. c) Average change in the circularity C for all inclusions during each deformation cycle, with circularity defined as $C = 4\pi \times Area\ Perimeter^{-2}$. d) Plot of the mean I_M/I_E ratio of all inclusions (closed circles) and the background signal (open circles) observed in CLSM images acquired at each deformation and relaxation step. For (a–d), solid lines serve as a guide to the eye. e) 3D models of the inclusions and their dominant emission color at the indicated deformation and relaxation steps (see Supporting Information for details). The x-, y-, and z-axes are the same as those referred to in (b).

acquisition, as evidenced by a decrease in inclusion brightness when re-imaging a previously irradiated spot of the film (Figure S14, Supporting Information) and by a decrease of the average inclusion I_M/I_E ratio with increasing irradiation time (Figure S15, Supporting Information). Moreover, both the overall image brightness and the I_M/I_E ratio were found to continuously decrease beyond a sample depth of ca. 30 µm (Figure S16, Supporting Information), which can, at least in part, be attributed to the more efficient transmission of lower-energy excitation light.[41] To avoid such imaging artifacts, all further CLSM measurements were carried out in the region between 5 and 20 µm below the sample surface, i.e., the region in which little depth-dependent variation in the I_M/I_E ratio was observed (Figure S16, Supporting Information). Moreover, the same, short acquisition time (ca. 2 min for 2D images and 5 min for 3D images of 40 µm-thick cross-sections) was used for all experiments, in order to minimize photo-bleaching.

To explore the effect of mechanical deformation on the inclusions, samples of PU/tOPV (1.0 wt.%) films were subjected to 3D CLSM imaging during uniaxial tensile deformation and subsequent relaxation at strains between 0 and 200% (see Supplementary Information for details). Images recorded at 200% strain show that the inclusions adopt an elongated, elliptical profile upon macroscopic sample deformation (Figure 2b[III–VI]). The analysis of the images confirms that the inclusions undergo the most significant shape change along the axis in which sam-

ple deformation occurs, indicated in the 3D CLSM image as the x-axis (Figure 2b[III]; Figure S17, Supporting Information). A quantitative comparison of the shape changes along the three main axes of the films (i.e., x, y, and z) during deformation (and relaxation) confirms that the elongation (and contraction) of inclusions occurs almost exclusively along the direction of sample deformation (**Figure 3**a,b). Moreover, the changes are fully reversible over at least two consecutive cycles of deformation and relaxation. These observations are corroborated via analysis of the 2D CLSM images, which reveals that the circularity of the inclusions corresponds inversely to the applied strain and is fully reversible (Figure 3a,c).

Changes in the fluorescence characteristics of the inclusions during mechanical deformation were further assessed by quantitatively comparing the emission intensities between 2D split-channel micrographs of a PU/tOPV (1.0 wt.%) film after performing a background subtraction to isolate individual inclusions. The average I_M/I_E ratio of the inclusions was found to correlate directly with the applied strain, increasing when the sample was stretched and decreasing when the stress was released (Figure 3a–d). The strain-dependent changes in the emission properties of the sub-micrometer inclusions are in excellent agreement with the previously reported macroscopic fluorescence response of the films,[20] which was determined by fluorescence spectroscopy (Figure S18, Supporting Information). The recorded spectra show maxima at 510 nm for the monomer and
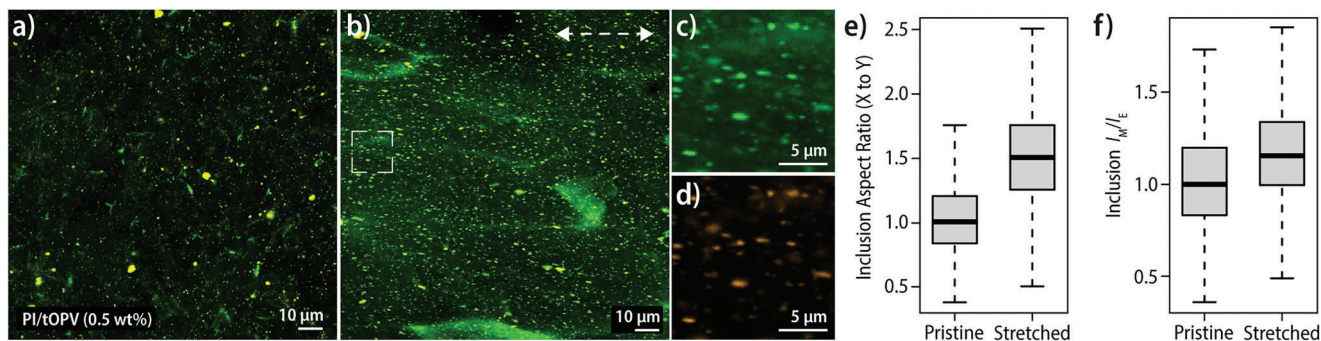
**ADVANCED
SCIENCE NEWS**

www.advancedsciencenews.com

**ADVANCED
FUNCTIONAL
MATERIALS**

www.afm-journal.de

Figure 4. a,b) CLSM images showing an overlay of the monomer and excimer emission channels for a PI/tOPV (0.5 wt.%) blend film (a) in the pristine, stress-free state and (b) after tensile deformation to ca. 280% strain (sample failure). Tensile deformation was applied with a microtensile tester at a strain rate of 50% min^{-1}. c,d) CLSM images showing (c) the monomer and (d) the excimer emission channel for the area indicated in (b) by a white square. e) Box plots showing the average aspect ratio, i.e., ratio between the lengths of the x- and y-axes of the inclusions in PI/tOPV (0.5 wt.%) blend films before and after tensile deformation. f) Box plots showing the average I_M/I_E ratio of the inclusions before and after tensile deformation. The bold horizontal lines represent the median values.

at 630 nm for the excimer, and the intensity ratio (I_{510}/I_{630}) determined in situ upon stretching and subsequent relaxation of samples linearly correlates with the applied strain. Some hysteresis is observed in the fluorescence response of the inclusions (Figure 3d), which likely arises from the high deformation rate and the limited relaxation time during CLSM imaging. As a matter of fact, a similar hysteresis is observed in the I_{510}/I_{630} monomer-to-excimer emission intensity ratio established by spectroscopic experiments on a PU/tOPV (1.0 wt.%) film that was deformed at a high strain rate of 250% min^{-1} and allowed to relax for 10 min (Figure S19, Supporting Information). Notably, no similar changes in the I_M/I_E ratio were observed for the background emission of the 2D CLSM images (Figure 3d), corroborating that the deformation of the sub-micrometer inclusions is in fact responsible for the macroscopic MRL behavior.

To confirm that this mechanism is also at play in other polymer matrices that feature tOPV as an additive, PI, PCL, and SBS blend films were investigated. Importantly, CLSM imaging reveals the presence of emissive sub-micrometer inclusions in PI/tOPV (0.5 wt.%) and PCL/tOPV (0.1 wt.%) blend films (**Figure 4**; Figures S20 and S21, Supporting Information). CLSM images of SBS/tOPV (1.0 wt.%) suggest inclusions are present, but with sizes <≈200 nm near the limit of optical resolution (Figure S22, Supporting Information), presumably due to a higher miscibility of the additive with SBS. Moreover, samples of PI/tOPV (0.5 wt.%) that were subjected to uniaxial tensile deformation show an elongation of the sub-micrometer-sized inclusions along the direction of sample deformation concomitant with an increase in the I_M/I_E ratio of the inclusions (Figure 4). These results mirror the bulk mechanofluorescent response previously demonstrated for these blend films[17] and thus unambiguously confirm that the formation of phase-separated inclusions of the additive is responsible for the highly sensitive mechanochromism observed for polymers that are blended with tOPV. It is moreover apparent that the strain-dependent response of tOPV blend films is derived primarily from changes in the shape of the additive inclusions as they deform in response to tensile strains applied to the polymer matrix.

To elucidate how changes in inclusion shape relate to applied strain and MRL behavior, an in-depth analysis was performed

with PU/tOPV (1.0 wt.%) films that were deformed in an equibiaxial manner in a custom-built device (see Supplementary Information for details). Equibiaxial deformation allows to apply strain uniformly without changing the sample position relative to the microscope's objective, which enables monitoring of individual inclusions by CLSM during mechanical deformation (Figure 5, Figures S23 and S24, Supporting Information). The recorded micrographs between strains of 0 and 135% show that equibiaxial deformation leads to an increase in the diameter of the inclusions and a concomitant flattening (Figures S25 and S26, Supporting Information). Analysis of the I_M/I_E ratio of individual inclusions shows a linear correlation with the applied strain (Figure 5g). These results mirror those obtained by bulk and microscopic analyses for uniaxially deformed samples and confirm that the MRL response arises due to the inclusions' deformation. In accordance with Eshelby's inclusion theory,[42,43] correlating the microscale deformation of the inclusions to the applied bulk strain allows one to derive their mechanical properties. To this end, radii (r_0) of individual inclusions prior to deformation and radii (r) of the same inclusions at different strains were determined to derive the stretch ratio (r/r_0). Plots of the average stretch ratio of the tOPV inclusions against the bulk strain (ϵ_B) show a linear relation (Figure 5h). The slope determined from a fit to the data (1.36) was found to be lower than predicted by Eshelby's theory for an incompressible liquid (2.50) and greater than for inclusions displaying the stiffness of the matrix (1.00). This finding indicates that the inclusions are solid, yet softer than the surrounding PU. The Young's modulus of pristine PU (19.8 MPa)[20] and the determined slope were used to establish the Young's modulus of the tOPV inclusions (E_i ≈6.7 MPa; see Equations S5–S7, Supporting Information).[42]

This analysis of individual inclusions was further validated by statistical processing of 3D CLSM images that were recorded at different equibiaxial strains. A bespoke MATLAB algorithm was used to find the centroid of each inclusion by fitting a Gaussian function to the emission intensity of the inclusion's brightest emission plane in the monomer channel (see Supporting Information for details). This allowed tracking the relative positions of up to 2000 inclusions per sample at different depths and to analyze their radii throughout equibiaxial deformation
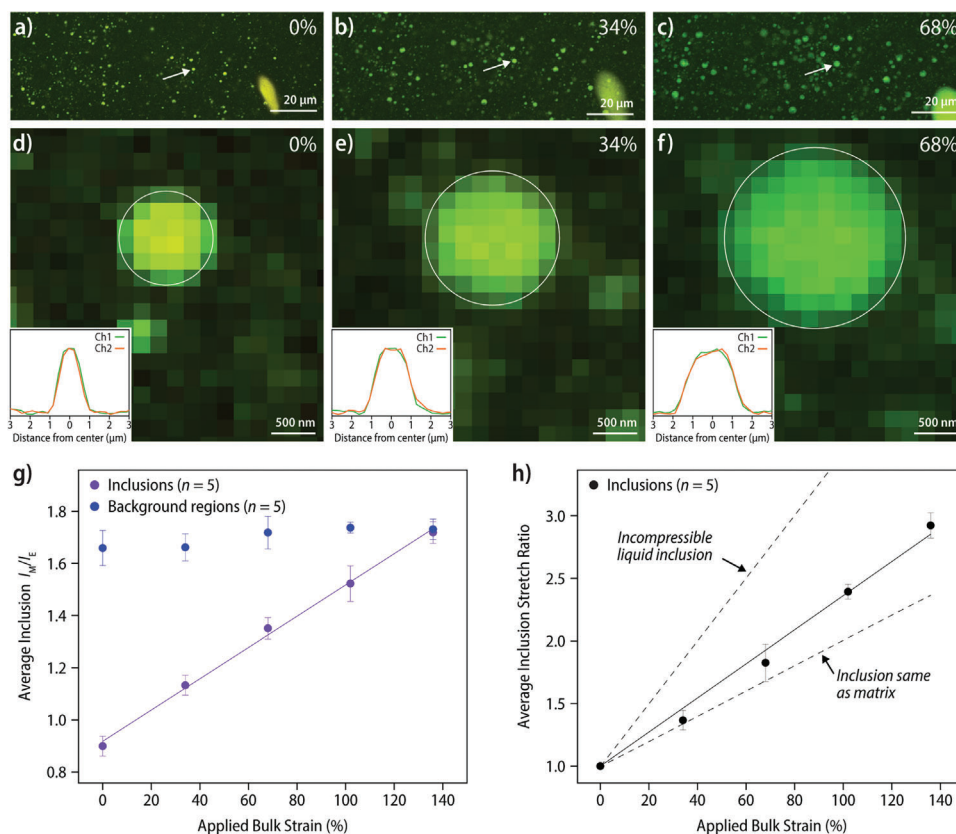
Figure 5. a–f) 2D CLSM images of a single inclusion in a PU/tOPV (1 wt.%) film subjected to equibiaxial deformation. (a–c) Arrows identify a single inclusion that is shown at higher magnification in (d–f). Insets in (d–f) show the normalized emission intensities in the monomer (Ch1) and excimer (Ch2) channels obtained by performing a line-scan through the center of the inclusion. g) Plot of the average I_M/I_E values as a function of the applied bulk strain for five individual inclusions (purple dots) and for the background region (blue dots). Error bars represent one standard deviation. h) Plot of the average stretch ratio (black dots) of the inclusions (i.e., radius r divided by the radius r_0 prior to deformation) as a function of the applied bulk strain. Dotted lines indicate limits predicted by Eshelby's theory for inclusions of different compressibility.[42,43]

experiments (Figure 5; Figure S24, Supporting Information). Plotting the stretch ratio (r/r_0) against the bulk strain (ϵ_b) for this large dataset yielded a slope of 1.41 and a resulting modulus of the inclusions of $E_i = 5.3$ MPa (Figure S27, Supporting Information), which matches excellently with the values obtained via manual analysis of individual inclusions. The determined modulus, together with the high degree of reversibility during cyclic uniaxial deformation experiments (Figure 2; Figure S17, Supporting Information), unambiguously confirms that the inclusions are elastic and act as efficient sensors for the applied bulk strain. Since these are Eshelby inclusions, strain is completely homogeneous inside the inclusions and independent of initial radius. In accordance with this analysis, the emission color at different strains is completely uniform across the whole inclusion (insets Figure 5d–f), affording the observed correlation between the macro- and microscopic mechanochromism. Moreover, the extent to which the fluorescence of individual inclusions changes in response to applied strain does not depend on the initial radius of the inclusion (Figure S28, Supporting Information), further corroborating the existence of a homogeneous strain field throughout the inclusions. To the best of our knowledge, the results presented herein constitute the first example of elastic inclusions formed by an aggregachromic additive that impart such

highly sensitive and reversible mechanochromism to different polymers.

We further sought to elucidate the process by which the inclusions form. To this end, the extent of dye aggregation was assessed by evaluating the inclusions' I_M/I_E ratio for a series of PU/tOPV samples with varying additive concentrations (**Figure 6**a,b). The analysis of CLSM images shows that the phase-separated inclusions display a decreasing I_M/I_E ratio, i.e., an enhanced excimer emission, with increasing additive concentration. While the emission from small inclusions that are prevalent in PU/tOPV samples with an additive concentration of 0.25 wt.% was difficult to assess, the average I_M/I_E ratio determined for individual inclusions in PU/tOPV films with higher additive concentrations (0.5–10 wt.%) is in excellent agreement with results from conventional fluorescence spectroscopy measurements on the bulk films (Figure 6a). Notably, both the bulk I_{510}/I_{630} and inclusion I_M/I_E ratios exhibit a sharp decrease when the additive concentration is increased to ca. 2 wt.%, beyond which the addition of more tOPV leads to a less pronounced change (Figure S29a, Supporting Information). Hence, above this concentration, the majority of the additives' dyes are aggregated in the inclusions. While a precise determination of the minimum tOPV content required to form the inclusions is impeded by the
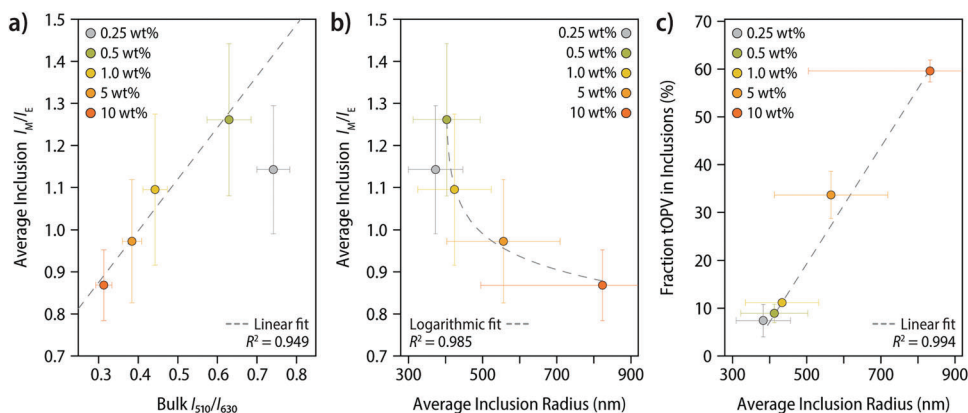
ADVANCED
SCIENCE NEWS

www.advancedsciencenews.com

ADVANCED
FUNCTIONAL
MATERIALS

www.afm-journal.de

Figure 6. a) Plot showing the correlation between the mean I_M/I_E ratio of the inclusions as determined from 3D CLSM images and the mean I_{510}/I_{630} ratio determined spectroscopically for bulk PU/tOPV (0.25–10 wt.%) blend films. b) Plot of the mean inclusion I_M/I_E ratio against the average inclusion radius as determined via Gaussian image analysis (Table S1, Supporting Information). It is worth noting that this analysis omits a significant number of smaller inclusions. c) Plot of the average internal fraction of the inclusions comprised of tOPV as determined from 2D CLSM image analysis against the average inclusion radius. For all plots, the grey dotted lines are linear or logarithmic fits of the data, and error bars represent one standard deviation.

fact that inclusions with radii near ca. 300 nm approach the optical resolution limit of the available CLSM setup, plots of the bulk I_{510}/I_{630} ratio against the tOPV concentration suggest that addition of as little as 0.1 wt.% of tOPV is sufficient (Figure S29b, Supporting Information).

In order to explore whether the extent of dye aggregation in the inclusions depends on inclusion size, the CLSM images of PU/tOPV (0.25–10 wt.%) blend films were assessed with the Gaussian fitting algorithm (vide supra). Notably, this analysis omits a significant number of smaller inclusions with radii on the order of a single pixel, which corresponds to ca. 130 nm. The analysis shows that the average size of the inclusions increases linearly with the amount of additive in the blend films, with the average inclusion radius increasing by ≈40 nm for every 1 wt.% of tOPV added (Figure S30a, Supporting Information). Notably, the inclusions' average I_M/I_E ratio decreases with increasing inclusion size and additive content in the series of PU/tOPV (0.5–10 wt.%) samples (Figure 6b), suggesting that larger inclusions contain more of the additive. Taken together, these relations and the determined mechanical properties suggest that the inclusions are not exclusively composed of the additive, but rather of a mixture of PU and tOPV. We hence analyzed PU/tOPV (0.25–10 wt.%) samples to establish the composition of the inclusions. To estimate the fraction of the tOPV additive in the inclusions, the pixel area belonging to the inclusions was divided by the total pixel area in the image, followed by normalization of the determined area fraction against the additive concentration (see Supporting Information for details). The analysis indicates that the composition drastically changes with the tOPV concentration, i.e., additive concentrations of 0.25, 0.5, 1, 5, and 10 wt.% furnish samples in which the inclusions are comprised of an estimated fraction of 7, 9, 11, 34, and 60% tOPV, respectively (Figure 6c; Figure S30b, Supporting Information). Such drastic differences in composition of the inclusions appears to stem from the highly disparate molecular weights of the additive (M_n = 4.5 kg mol^{-1}) and the polymer matrices (M_n = 80–400 kg mol^{-1}), in contrast to the predominantly single-component phases expected for immiscible polymers of similar molecular weight.[44]

Taken together, the results corroborate that an increase of tOPV content in the blend films leads to the formation of larger inclusions that contain a higher fraction of the additive (Figure 6c; Tables S1–S4, Supporting Information). It furthermore becomes clear when grouping inclusions by size that the observed trends hold both for inclusions with different sizes in samples with a given tOPV concentration (Figures S32 and S33 and Tables S5−S9, Supporting Information) as well as across samples with different concentrations (Figure 6b). Thus, with increasing additive concentration, the arrangement of molecules within individual inclusions appears to approach that of neat tOPV with a high degree of excimer emission (Figure S34, Supporting Information).

Finally, we probed the effect of matrix composition on the formation of inclusions by applying the same Gaussian fitting algorithm and image masking protocol to PI/tOPV (0.5 wt.%) and PCL/tOPV (0.1 wt.%) blend films. The results show that inclusions in these samples exhibit average radii of 433 ± 188 and 480 ± 176 nm, as well as average I_M/I_E ratios of 1.28 ± 0.37 and 0.51 ± 0.18, respectively (Table S1 and S2, Supporting Information). Moreover, the internal fraction of the inclusions comprised of tOPV was determined to be on the order of 8.1 ± 0.5% for PI/tOPV (0.5 wt.%) and 3.6 ± 0.4% for PCL/tOPV (0.1 wt.%) samples (Figure S31, Supporting Information). Thus in PI/tOPV (0.5 wt.%), the inclusions' size, composition, and extent of excimer formation resembles that of inclusions in PU/tOPV (0.5 wt.%) samples, suggesting a similar miscibility of the additive in these respective matrices. On the other hand, when PCL is used as matrix, the inclusions that form are larger, and the dyes have a greater tendency to aggregate within these inclusions. Interestingly, inclusions in PCL appear to contain fivefold less tOPV than inclusions of the same size in PU (Figure 6c), pointing to a different miscibility and phase-separation kinetics that may derive from the crystallinity of the matrix. The formation of the inclusions, hence, appears to correlate with the miscibility of the additives' polymer backbone and the matrix. On the other hand, the dye association into excimers is an independent process, which relies on attractive molecular interactions.

The results reported herein demonstrate that the formation of phase-separated inclusions is essential for the mechanochromism displayed by the tOPV additive, and that the macromolecular nature of the additive plays a key role in the formation of these inclusions. The process occurs in a variety of polymer matrices (e.g., PU, PI, PCL, and SBS), rendering the use of macromolecular additives considerably more versatile than conventional small-molecule dye blending approaches toward mechanochromic materials. Indeed, experiments with PU and an untethered small-molecule oligo(p-phenylene vinylene) dye (Figure S1, Supporting Information)[33,45] show that exclusively large dye aggregates (20–50 μm) are formed, which remain intact upon deformation (Figure S37, Supporting Information). On the other hand, blending a dye derivative that does not feature extended alkyl terminal groups (Figure S1, Supporting Information)[45] into a commodity linear low-density polyethylene (LLDPE) polymer yields aggregates ≈1–5 μm in size; deformation to 500% strain in this case significantly reduces the number of aggregates and a significant monomer emission is observed (Figure S38, Supporting Information), corroborating previous findings that blends of LLDPE with these dye molecules are highly, but irreversibly, mechanochromic.[46] These examples serve to illustrate that, in contrast to the use of macromolecular additives, the small-molecule dye blending strategy is effective only for selected combinations of polymers and aggregachromic dyes.

3. Conclusion

Different types of polymers can be endowed with a highly sensitive, strain-dependent, and reversible MRL response when blended with small quantities of a telechelic macromolecule carrying excimer-forming cyano-OPV dyes. We demonstrate that this mechanochromism stems from emissive Eshelby inclusions, which form during the blending process due to the (limited) miscibility between the additive's polymeric backbone and the surrounding polymer matrix. Our analysis shows that the inclusions consist of a combination of the matrix polymer and the additive. As a result, the mechanical properties of the inclusions are closely tied to those of the surrounding matrix. This suggests that efficient force transfer between the two components is mediated by chain entanglements between the additive's polymer backbone and the matrix. At the molecular level, the weak attractive interactions between the dye molecules of the additive lead to the formation of mechanically sensitive excimers, ensuring that even small mechanical forces can cause the dye pairs to dissociate. Indeed, our in situ analysis during sample deformation shows that macroscopic tensile deformation of the polymer blends induces changes in both the shape and emission of the inclusions, indicating that a reversible (dis)aggregation of the cyano-OPV dyes occurs within the inclusions. The uniform force field within the Eshelby inclusions results in a consistent change in emission color that is proportional to the extent of deformation and relaxation through multiple cycles. This holds true on both the individual inclusion level as well as macroscopically.

The fact that polymer materials are rendered mechanochromic by blending very low quantities of an additive without the need for synthetic modifications renders the strategy highly versatile and readily compatible with industrial processing protocols. The additive investigated in this study already allows to create mechanochromic materials from a broad range of polymers. However, modifying the additive's polymeric backbone and dye molecules should allow to tailor the size and composition of the inclusions, as well as their MRL response. As a result, this approach can be easily adapted to a wide range of polymers, making it possible to customize the force response within any given (polymer) matrix. More generally, mechanochromic inclusions constitute a new paradigm for visualizing the transfer of bulk forces from the macro- to the nanoscale, and we believe that the detailed mechanistic insights presented herein will facilitate the development of new and effective MRL materials.

Supporting Information

Supporting Information is available from the Wiley Online Library or from the author.

Conflict of Interest

The authors declare no conflict of interest.

Author Contributions

D.J.K., C.W., and S.S. developed the original concept for the study and designed the materials and experiments. D.J.K. fabricated the PU blend films, characterized all materials, and performed the experiments. R.S. and D.V. analyzed the CLSM images together with D.J.K. C.C. synthesized the tOPV additive and fabricated the PCL, PI, and SBS blend films. All authors discussed the results and contributed to the interpretation of the data. D.J.K., C.W., and S.S. wrote the paper. All authors contributed to editing of the manuscript.

Data Availability Statement

The datasets generated and analyzed during the current study are available from the corresponding author on reasonable request. The source data generated during this study are available at the Zenodo repository at: https://doi.org/10.5281/zenodo.8211012.

[1] C. Calvino, L. Neumann, C. Weder, S. Schrettl, *J. Polym. Sci., Part A: Polym. Chem.* **2017**, *55*, 640.

[2] J. Li, C. Nagamani, J. S. Moore, *Acc. Chem. Res.* **2015**, *48*, 2181.

[3] O. Rifaie-Graham, E. A. Apebende, L. K. Bast, N. Bruns, *Adv. Mater.* **2018**, *30*, 1705483.

[4] H. Traeger, D. J. Kiebala, C. Weder, S. Schrettl, *Macromol. Rapid Commun.* **2021**, *42*, 2000573.

[5] C. Weder, in *Encyclopedia of Polymeric Nanomaterials*, Springer, Berlin, Heidelberg **2013**.

[6] Y. Chen, G. Mellot, D. van Luijk, C. Creton, R. P. Sijbesma, *Chem. Soc. Rev.* **2021**, *50*, 4100.

[7] C. M. Geiselhart, H. Mutlu, C. Barner-Kowollik, *Angew. Chem., Int. Ed.* **2021**, *60*, 17290.

[8] P. Cawley, *Struct. Health Monit.* **2018**, *17*, 1225.

[9] T. Magrini, D. Kiebala, D. Grimm, A. Nelson, S. Schrettl, F. Bouville, C. Weder, A. R. Studart, *ACS Appl. Mater. Interfaces* **2021**, *13*, 27481.

[10] M. K. Beyer, H. Clausen-Schaumann, *Chem. Rev.* **2005**, *105*, 2921.

[11] M. M. Caruso, D. A. Davis, Q. Shen, S. A. Odom, N. R. Sottos, S. R. White, J. S. Moore, *Chem. Rev.* **2009**, *109*, 5755.

[12] M. Stratigaki, R. Göstl, *ChemPlusChem* **2020**, *85*, 1095.

[13] G. Chen, W. Hong, *Adv. Opt. Mater.* **2020**, *8*, 2000984.

[14] J. M. Clough, C. Weder, S. Schrettl, *Macromol. Rapid Commun.* **2021**, *42*, 2000528.

[15] M. Raisch, W. Maftuhin, M. Walter, M. Sommer, *Nat. Commun.* **2021**, *12*, 4243.

[16] H. Hu, X. Cheng, Z. Ma, R. P. Sijbesma, Z. Ma, *J. Am. Chem. Soc.* **2022**, *144*, 9971.

[17] C. Calvino, Y. Sagara, V. Buclin, A. P. Haehnel, A. del Prado, C. Aeby, Y. C. Simon, S. Schrettl, C. Weder, *Macromol. Rapid Commun.* **2019**, *40*, 1800705.

[18] Y. Chen, C. J. Yeh, Y. Qi, R. Long, C. Creton, *Sci. Adv.* **2020**, *6*, eaaz5093.

[19] E. Ducrot, Y. Chen, M. Bulters, R. P. Sijbesma, C. Creton, *Science* **2014**, *344*, 186.

[20] D. J. Kiebala, Z. Fan, C. Calvino, L. Fehlmann, S. Schrettl, C. Weder, *Org. Mater.* **2020**, *02*, 313.

[21] J. Slootman, V. Waltz, C. J. Yeh, C. Baumann, R. Göstl, J. Comtet, C. Creton, *Phys. Rev. X* **2020**, *10*, 041045.

[22] F. Yang, Y. Yuan, R. P. Sijbesma, Y. Chen, *Macromolecules* **2020**, *53*, 905.

[23] R. Kotani, S. Yokoyama, S. Nobusue, S. Yamaguchi, A. Osuka, H. Yabu, S. Saito, *Nat. Commun.* **2022**, *13*, 303.

[24] M. J. Robb, W. Li, R. C. R. Gergely, C. C. Matthews, S. R. White, N. R. Sottos, J. S. Moore, *ACS Cent. Sci.* **2016**, *2*, 598.

[25] C. Calvino, A. Guha, C. Weder, S. Schrettl, *Adv. Mater.* **2018**, *30*, 1704603.

[26] M. Stratigaki, C. Baumann, L. C. A. van Breemen, J. P. A. Heuts, R. P. Sijbesma, R. Göstl, *Polym. Chem.* **2020**, *11*, 358.

[27] T. Yamakado, S. Saito, *J. Am. Chem. Soc.* **2022**, *144*, 2804.

[28] C. Löwe, C. Weder, *Adv. Mater.* **2002**, *14*, 1625.

[29] A. Pucci, G. Ruggeri, *J. Mat. Chem.* **2011**, *21*, 8282.

[30] F. Ciardelli, G. Ruggeri, A. Pucci, *Chem. Soc. Rev.* **2013**, *42*, 857.

[31] S. Schrettl, D. W. R. Balkenende, C. Calvino, M. Karman, A. Lavrenova, L. N. Neumann, Y. Sagara, E. Verde-Sesto, M. di Giannantonio, Y. C. Simon, K. M. Fromm, M. Lattuada, C. Weder, *Chimia* **2019**, *73*, 7.

[32] B. R. Crenshaw, M. Burnworth, D. Khariwala, A. Hiltner, P. T. Mather, R. Simha, C. Weder, *Macromolecules* **2007**, *40*, 2400.

[33] B. R. Crenshaw, C. Weder, *Macromolecules* **2006**, *39*, 9581.

[34] H. Traeger, Y. Sagara, D. J. Kiebala, S. Schrettl, C. Weder, *Angew. Chem., Int. Ed.* **2021**, *60*, 16191.

[35] C. Micheletti, V. A. Dini, M. Carlotti, F. Fuso, D. Genovese, N. Zaccheroni, C. Gualandi, A. Pucci, *ACS Appl. Polym. Mater.* **2023**, *5*, 1545.

[36] C. Calvino, E. Henriet, L. F. Muff, S. Schrettl, C. Weder, *Macromol. Rapid Commun.* **2020**, *41*, 1900654.

[37] C. Calvino, C. Weder, *Small* **2018**, *14*, 1802489.

[38] J. Kunzelman, B. R. Crenshaw, M. Kinami, C. Weder, *Macromol. Rapid Commun.* **2008**, *27*, 1981.

[39] M. Rubinstein, R. H. Colby, *Polymer Physics*, Oxford University Press, Oxford, New York **2003**.

[40] B. R. Masters, M. A. Farmer, *Comput. Med. Imaging Graph* **1993**, *17*, 211.

[41] D. Wang, M. Wagner, H. J. Butt, S. Wu, *Soft Matter* **2015**, *11*, 7656.

[42] R. W. Style, R. Boltyanskiy, B. Allen, K. E. Jensen, H. P. Foote, J. S. Wettlaufer, E. R. Dufresne, *Nat. Phys.* **2015**, *11*, 82.

[43] J. D. Eschelby, *Proc. R. Soc. London, Ser. A* **1957**, *241*, 376.

[44] R. Koningsveld, W. H. Stockmayer, E. Nies, *Polymer Phase Diagrams: A Textbook*, Oxford University Press, Oxford, New York **2001**.

[45] M. Kinami, B. R. Crenshaw, C. Weder, *Chem. Mater.* **2006**, *18*, 946.

[46] B. R. Crenshaw, C. Weder, *Chem. Mater.* **2003**, *15*, 4717.